



Therapeutic potential of the neutralizing monoclonal antibody 45G3 against encephalomyocarditis virus

Yanfang Zhang^{1,2,3,4,5}, Zhiying Wang⁵, Yaohui Fang⁵, Qiong Zhu⁵, Jie Fu⁵, Sijing Hu⁵, Jiayin Jin⁵, Min Zhou⁵, Xijia Liu⁵, Danna Zhang⁵, Shouwei Huang⁵, Yali Deng⁵, Lingling Xie⁵, Shu Shen⁵, Jing Ye^{1,2,3,4}, Fei Deng^{5*} and Shengbo Cao^{1,2,3,4*}

Abstract

Encephalomyocarditis virus (EMCV), a potential zoonotic pathogen, poses significant socioeconomic and public health challenges across various host species. Although EMCV rarely triggers severe clinical symptoms in humans, its widespread prevalence and unique biological characteristics underscore the need for continuous surveillance and the development of effective therapeutics and prophylactics. In this study, we evaluated the neutralizing effects of a monoclonal antibody derived from the spleens of mice immunized with EMCV virus-like particles (VLPs), both in vitro and in vivo. Using recombinant DNA technology, we engineered a baculovirus system to express EMCVs P12A and 3C, facilitating the production of VLPs in Sf9 cells. These VLPs serve as antigens to immunize mice, leading to the isolation of the monoclonal antibody 45G3. This antibody exhibited high specificity for EMCV conformational epitopes, excluding linear epitopes, and demonstrated potent in vitro neutralizing activity, with an IC50 of 0.01873 µg/mL. Immunoelectron microscopy (IEM) revealed a strong direct interaction between the 45G3 antibody and EMCV particles. Virus adsorption inhibition assays demonstrated that 45G3 effectively blocked viral attachment, thereby preventing further infection of host cells. These findings further support the notion of a robust interaction between the virus and the antibody. Moreover, in vivo assessments revealed that 45G3 significantly reduced viral loads in treated mice and improved survival outcomes following EMCV exposure. Additionally, posttreatment analysis revealed reduced tissue damage and a markedly decreased inflammatory response in the brain, indicating that the 45G3 antibody effectively blocked viral infection, thereby mitigating tissue damage and enhancing survival. These findings position 45G3 as a promising candidate for EMCV management and provide a strong foundation for the future development of antiviral drugs targeting this widespread virus.

Keywords Encephalomyocarditis virus, Monoclonal antibody, Virus-like particles, Neutralizing activity, Therapeutic efficacy, Antiviral development

Handling editor: Fang He.

*Correspondence:

Fei Deng

df@wh.iov.cn

Shengbo Cao

sbcao@mail.hzau.edu.cn

Full list of author information is available at the end of the article

Introduction

EMCV is the causative agent of zoonotic diseases characterized primarily by encephalitis and myocarditis (Carocci and Bakkali-Kassimi 2012). EMCV was initially discovered in a gibbon in Florida in 1945 (Helwig and Schmidt 1945), followed by its isolation from pigs after a Panama epizootic in 1958 (Murnane et al. 1960).



© The Author(s) 2025. **Open Access** This article is licensed under a Creative Commons Attribution 4.0 International License, which permits use, sharing, adaptation, distribution and reproduction in any medium or format, as long as you give appropriate credit to the original author(s) and the source, provide a link to the Creative Commons licence, and indicate if changes were made. The images or other third party material in this article are included in the article's Creative Commons licence, unless indicated otherwise in a credit line to the material. If material is not included in the article's Creative Commons licence and your intended use is not permitted by statutory regulation or exceeds the permitted use, you will need to obtain permission directly from the copyright holder. To view a copy of this licence, visit <http://creativecommons.org/licenses/by/4.0/>. The Creative Commons Public Domain Dedication waiver (<http://creativecommons.org/publicdomain/zero/1.0/>) applies to the data made available in this article, unless otherwise stated in a credit line to the data.

Since its first identification, EMCV has been recognized in a broad spectrum of wild and domesticated species worldwide, including Europe (Canelli et al. 2010; Cardeti et al. 2016), Canada (Dea et al. 1991), South America (Czechowicz et al. 2011), Australia (Reddacliff et al. 1997), Korea (An et al. 2009), and China (Ge et al. 2010). The virus has been identified in diverse species, including voles, squirrels, elephants, pigs, wild boars, raccoons, antelopes, lions, various birds, and numerous primates (Billinis 2009; Canelli et al. 2010; Cardeti et al. 2016; Gainer 1967; Luo et al. 2017; Medkour et al. 2021; O'Connor et al. 2020; Romey et al. 2021; Vyshemirskii et al. 2018). Infection in pigs leads to acute myocarditis and sudden death, especially in young piglets (Gelmetti et al. 2006), with mortality rates sometimes reaching 100%. Furthermore, the reproductive health of pregnant sows is severely compromised, often resulting in miscarriage, stillbirth, and the birth of weak offspring (Salogni et al. 2016; Vansteenkiste et al. 2016). Rodents, which act as natural reservoirs, play a pivotal role in the epidemiology of EMCV (Camp and Desvars-Larrive 2022), aiding its persistence and transmission primarily through the fecal–oral route via contaminated food and water (Gainer 1967). This mode of transmission significantly affects pig populations, as evidenced by serological surveys revealing widespread infections in pig farms, especially in regions such as China (Feng et al. 2015; Liu et al. 2016).

EMCV is a nonenveloped, single-stranded RNA virus classified within the *Cardiovirus* genus of the Picornaviridae family (Palmenberg et al. 1984). The EMCV genome is approximately 7.8 kb in length and is organized into a single open reading frame that encodes a polyprotein. This polyprotein undergoes posttranslational cleavage to yield structural and nonstructural viral proteins essential for viral replication, assembly, and pathogenicity (Carocci and Bakkali-Kassimi 2012; Foglia et al. 2023). Structural proteins, including VP1, VP2, VP3 and VP4, form the viral capsid and play critical roles in host cell receptor binding and entry, whereas nonstructural proteins, such as 2A, 2B, 2C, 3A and 3B (VPg) (Guo et al. 2021; Han et al. 2021), 3C protease, and 3D polymerase, are involved in the replication complex and polyprotein processing (Carocci and Bakkali-Kassimi 2012; Carocci et al. 2011; Cherry 2019; Han et al. 2022, 2021; Huang et al. 2017; Zoll et al. 1998).

In the field of disease prevention and control caused by pathogens, the discovery and application of antibodies are key factors for effective interventions. Recent studies have focused on specific antibodies against various viruses, particularly neutralizing antibodies, because they can directly block the infection process. Research on

SARS-CoV-2 has revealed the existence of specific neutralizing antibodies that can bind to the receptor-binding domain of the virus and prevent its entry into host cells (Tang et al. 2022). Specifically, the combined use of four antibodies targeting the conserved regions of the receptor-binding domain and the stem helix structure can effectively prevent escape mutations. This further underscores the potential of neutralizing antibodies in controlling the spread of epidemics. In the development of viral vaccines, similar strategies have been successfully applied to foot-and-mouth disease virus (FMDV), a closely related picornavirus. FMDV is a significant pathogen in livestock, and while inactivated vaccines have been the traditional approach, recombinant vaccines offer the advantage of differentiating infected from vaccinated animals without the use of live virus. One such strategy involves the use of recombinant P1-2A-3C constructs to produce virus-like particles (VLPs) in Sf9 cells (Mohana Subramanian et al. 2012). These VLPs, when combined with an oil adjuvant, have been shown to induce strong immune responses in cattle, including the generation of high neutralizing antibody titers. Another approach involves the in vitro assembly of VLPs from the FMDV capsid proteins VP1, VP2 and VP3, which has proven effective in eliciting robust immune responses in animal models (Wang et al. 2023). These vaccine strategies have demonstrated the potential to provide broad protection and offer valuable insights into the design of similar vaccines for other viruses, including EMCV. The studies mentioned above demonstrate that VLPs not only serve as promising vaccine candidates for the prevention and control of diseases but also play crucial roles in the generation of neutralizing antibodies. Currently, there are no specific treatment options available for EMCV, nor are any neutralizing antibody products available on the market. Therefore, research on neutralizing antibodies against EMCV may provide new insights and strategies for treating this disease.

Collectively, these investigations indicate that EMCV is globally distributed and can infect an extensive variety of animal species, indicating that it has considerable potential for zoonotic transmission. Therefore, it is necessary to develop effective prevention and control measures against EMCV. Recent advances in monoclonal antibody (mAb) technology have opened new avenues for antiviral therapy, offering specificity, high efficacy, and reduced side effects compared with conventional treatments. This study focused primarily on isolating a neutralizing monoclonal antibody from the spleens of mice immunized with EMCV VLPs. We evaluated the neutralizing effects both in vitro and in vivo and demonstrated excellent neutralization and protective efficacy in both settings. Further evidence from viral load measurements

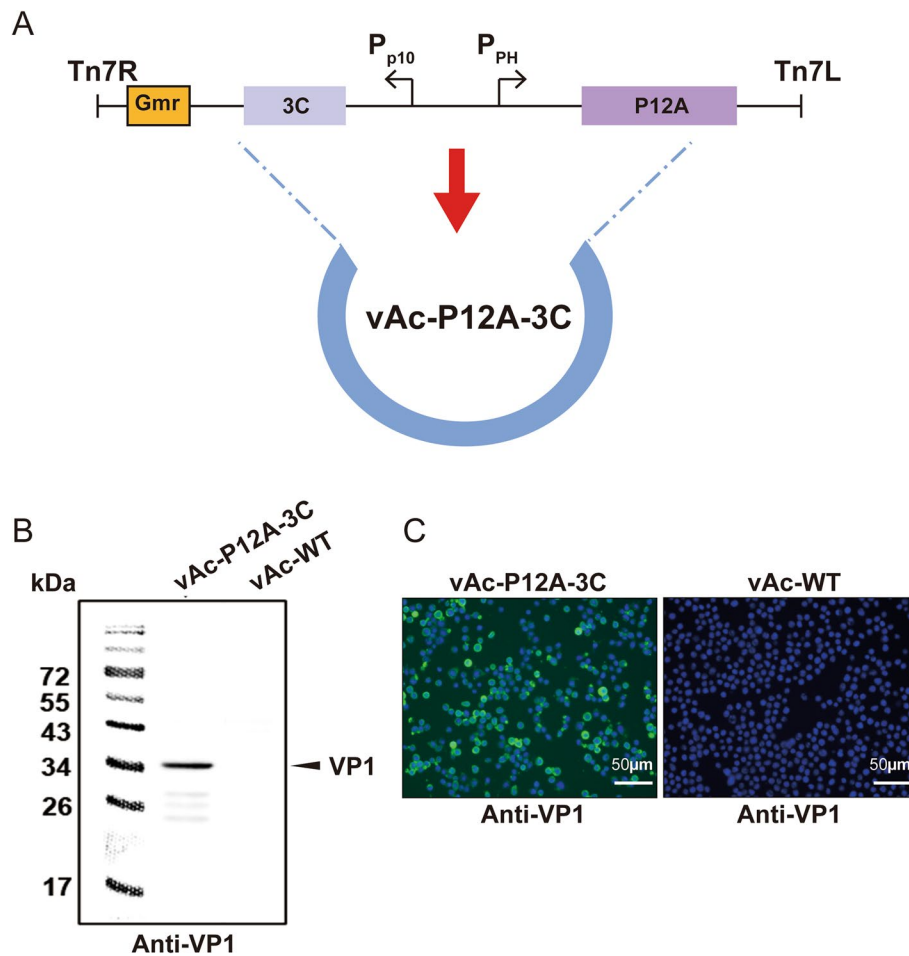


Fig. 1 Construction, expression and identification of EMCV-VLPs. Note: **A.** Construction diagram of Ac-P12A-3C; **B.** Identification of Ac-P12A3C by western blot analysis. Lane 1 represents Sf9 cells infected with Ac-P12A-3C recombinant baculovirus; lane 2 represents Sf9 cells infected with Ac-WT; **C.** Identification of Sf9 cells infected with Ac-P12A-3C recombinant baculoviruses via IFA, bar: 50 μ m. The primary antibody used was a monoclonal antibody, Anti-VP1, which was independently selected following the immunization of mice with VP1 expressed in a prokaryotic system

and pathological sections confirmed that the neutralizing antibody reduced viral loads in various tissues and mitigated pathological damage. The development of such mAbs not only provides a critical tool for combating EMCV infections but also contributes to our understanding of viral pathogenesis, paving the way for novel antiviral interventions.

Results

Recombinant baculovirus expressing EMCV Ac-P12A-3C

The recombinant bacmid vAc-P12A-3C were constructed by inserting the genes encoding EMCV 3C and P12A into the AcMNPV bacmid under the control of the p10 and polyhedrin promoters, respectively (Fig. 1A). After transfection, the Sf9 cells were infected with the Ac-P12A-3C recombinant virus (multiplicity of infection

of 1) for 72 h. Western blot (WB) analysis of the cell lysates revealed that the VP1 monoclonal antibody produced a protein band of approximately 35 kDa, which was consistent with the expected size of the VP1 protein, indicating that the precursor protein P1 was correctly expressed and cleaved (Fig. 1B). Indirect immunofluorescence analysis revealed significant green fluorescence signals in Sf9 cells infected with Ac-P12A-3C (Fig. 1C), further confirming the successful expression of VP1.

Recombinant baculovirus expressing P12A and 3C in EMCV generated VLPs

To investigate whether the P1 protein can self-assemble into VLPs after being cleaved by the 3C protein, Sf9 cells infected with the Ac-P12A-3C recombinant virus at 72 h post infection were fixed and observed via TEM.

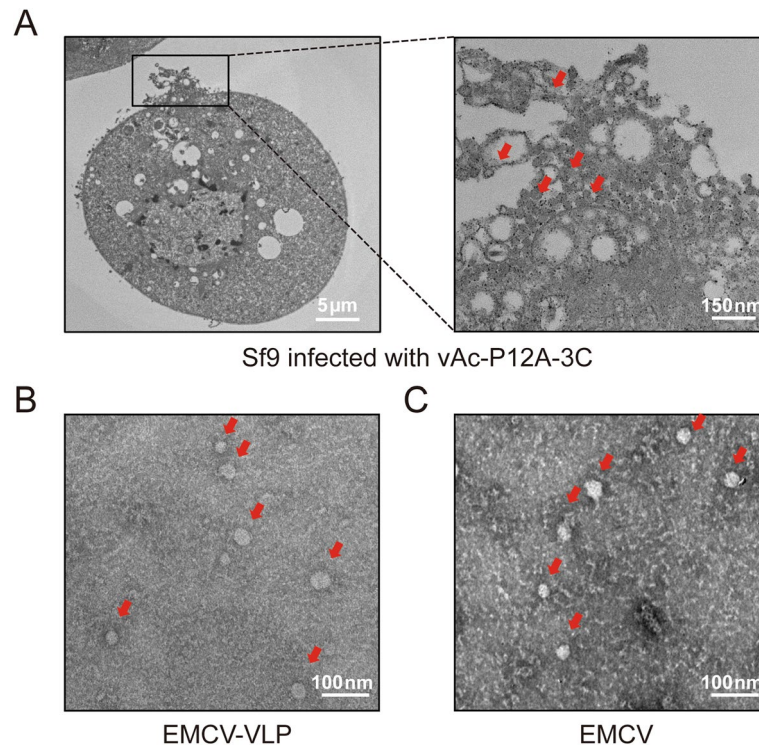


Fig. 2 Detection of EMCV-VLPs via transmission electron microscopy (TEM). Note: **A.** Electron microscopy images of Sf9 cells infected with the recombinant baculovirus vAc-P12A-3C; **B.** Negative electron microscopy images of EMCV VLPs; **C.** Negative electron microscopy images of EMCV. The EMCV and EMCV VLPs were both homogeneous spherical particles with a diameter of approximately 30 nm. Bar, 100 nm;

As shown in Fig. 2A, spherical particles approximately 30 nm in diameter with a uniform size and regular morphology were observed in the vesicle structure outside the cell membrane, similar to virus exocytosis.

To further determine the morphological characteristics of the VLPs, the cell lysates were purified via cesium chloride (CsCl) density gradient centrifugation. A dense white band between CsCl densities of 1.2 g/cm³ and 1.4 g/cm³ was collected, desalted, and prepared as negatively stained samples for TEM observation. As shown in Fig. 2B, uniform spherical particles of approximately 30 nm in diameter were observed via TEM, which were consistent with those of the live virus particles (Fig. 2C).

Anti-EMCV monoclonal antibody (45G3) identified from VLP-immunized BALB/c Mice directly interacts with EMCV

After three subcutaneous administrations of EMCV-VLPs in mice, a monoclonal antibody, designated 45G3, was isolated via hybridoma fusion technology. Subsequent indirect immunofluorescence assays demonstrated a robust interaction between the 45G3 mAb and EMCV-infected Vero cells, as well as vAc-P12A-3C-infected Sf9 cells (Fig. 3A). Conversely, WB analysis using EMCV-infected Vero cells and vAc-P12A-3C-infected Sf9 cells as

the antigen and 45G3 mAb as the primary antibody failed to reveal bands (Fig. 3B), indicating that the 45G3 mAb does not bind to the linear epitopes but rather to the conformational epitopes of EMCV proteins. ELISAs coated with virus-like particles (VLPs) were used to assess the effects of the 45G3 antibody, revealing that the optical density (OD₄₅₀) values across various antibody concentrations were significantly greater than those of the PBS control group. Linear regression analysis revealed a significant correlation between 45G3 and VLP ($P=0.04$), confirming an interaction between the EMCV VLP and the antibody (Supplementary Material, Figure S1).

The direct interaction between the EMCV and the antibody was confirmed via immunoelectron microscopy. Under a 200 kV electron microscope, a distinct ring of 6 nm gold particles surrounding the viral particles was observed when the 45G3 antibody was used as the primary antibody. In contrast, when mouse IgG was used as the primary antibody, gold particles were scattered throughout the field and did not accumulate around the viral particles. These results provide evidence that the 45G3 antibody directly interacts with the EMCV (Fig. 3C).

To identify the target protein of 45G3, we expressed EMCV proteins (VP1, VP2, VP3, VP4, 2A and 3C) in

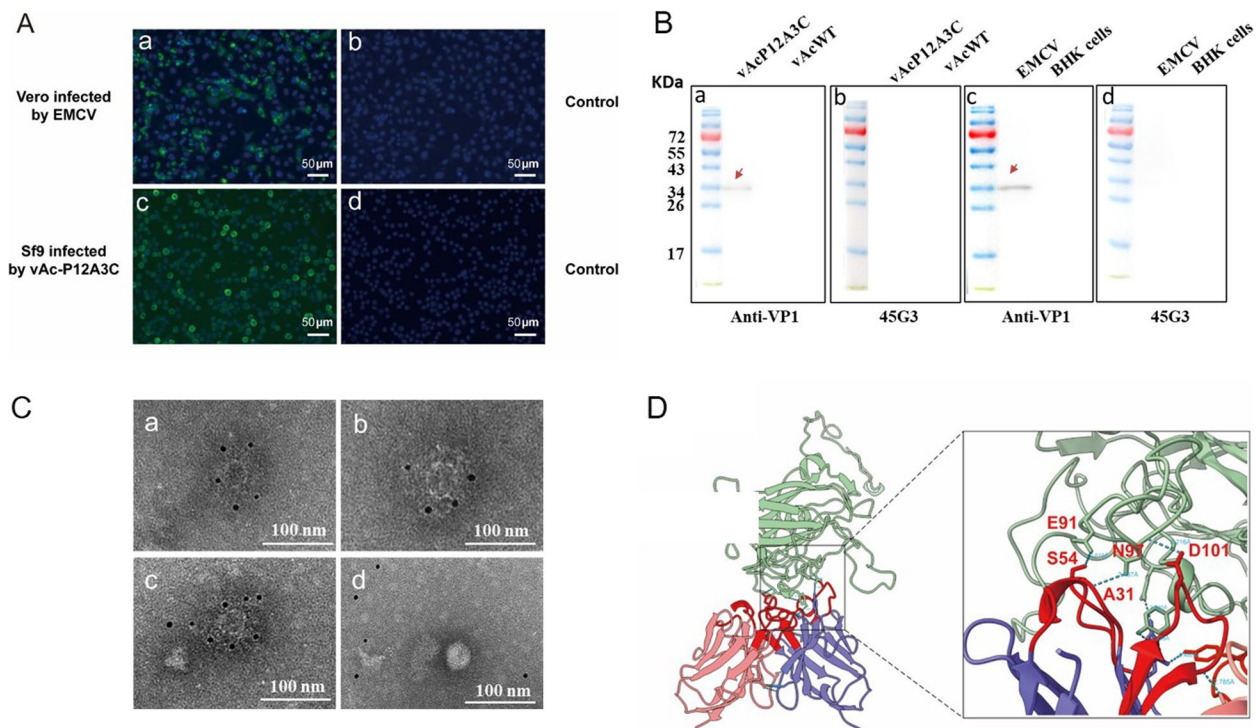


Fig. 3 Identification and characterization of mAbs against EMCV. Note: **A.** Identification of 45G3 in Vero cells infected with EMCV and Sf9 cells infected with Ac-P12A-3C recombinant baculoviruses *via* IFA; bar: 50 μ m. **B.** Identification of 45G3 in Vero cells infected with EMCV and Sf9 cells infected with Ac-P12A-3C recombinant baculoviruses *via* Western blotting. In Figures a and b, Sf9 cells were infected with Ac-P12A-3C (lane 1) and wild-type *Acanthamoeba castellanii* virus (WtAc, lane 2), respectively. Western blot analysis was conducted using a custom-made anti-VP1 monoclonal antibody (figure a) and a 45G3 antibody (figure b) to detect the presence of the VP1 protein. A distinct band at approximately 35 kDa, indicative of VP1 expression, was observed in both figures and is marked with a red arrow. Similarly, in Figures c and d, BHK cells were infected with EMCV (lane 1) or served as uninfected controls (lane 2). Western blot analysis was performed using the same custom-made anti-VP1 monoclonal antibody (figure c) and the 45G3 antibody (figure d). A band corresponding to the expected size of VP1 (35 kDa) was detected in both infected cell lysates, as indicated by the red arrow. These findings confirm the specific and successful expression of the VP1 protein in virus-infected cells. **C.** Immunoelectron microscopy (IEM) detection. In figures a, b, and c, the primary antibody used for immunostaining was 45G3, which was applied at a dilution of 1:100 to ensure optimal binding specificity and sensitivity. Conversely, in figure d, a mouse IgG antibody served as the primary antibody used as a control. **D.** 3D binding epitopes predicted by AlphaFold. Green: VP1, pink: H1, and purple: K1. The red regions indicate the antibody variable regions, with the amino acids at the interaction sites marked

eukaryotic systems and tested their interactions with 45G3 through an immunofluorescence assay (IFA) (Supplementary Material, Figure S2) and Western blot (WB) (Supplementary Material, Figure S3). However, no interactions were detected, suggesting that the epitope recognized by 45G3 likely involves a complex conformational structure not preserved in isolated protein forms. These findings confirm that 45G3 specifically blocks EMCV by targeting a conformational epitope.

To investigate the antigen epitope recognized by mAb 45G3, we obtained sequences of the hybridoma cell antibody variable regions H2 and K2. Using AlphaFold 3, a three-dimensional interaction model of these variable regions with VP1 was constructed (Fig. 3D). The types and strengths of the protein–protein interactions were then evaluated *via* PDBePISA. The results showed that

both H2 and K2 of mAb 45G3 interacted with viral VP1 (Table 1), forming hydrogen bonds at the E91, N97 and D101 sites of VP1 (Fig. 3D). This interaction may explain the neutralizing activity of the mAb 45G3.

The 45G3 antibody has neutralizing activity and effectively inhibits viral adsorption.

To assess the neutralizing activity of the 45G3 antibody, we determined its IC₅₀ *in vitro* *via* a plaque reduction neutralization assay. The results showed that the mAb 45G3 effectively neutralized EMCV, with the half-maximal inhibitory concentration (IC₅₀) calculated to be approximately 0.01873 μ g/mL (Fig. 4A). Another method to detect the half-maximal inhibitory concentration (IC₅₀) was calculated to be approximately 0.2096 μ g/mL *via* a 96-well plate microcell culture method in conjunction with an immunofluorescence assay (IFA) and

Table 1 PISA Interface List

Type	Mol 1				Mol 2				Interface area, Å ^{2d}	Δ ⁱ G kcal/mol ^e	Δ ⁱ G P-value ^f
	Range	ⁱ N _{at} ^a	ⁱ N _{res} ^b	Surface Å ^{2c}	Range	ⁱ N _{at}	ⁱ N _{res}	Surface Å ²			
1	45G3-H2	101	23	6623	45G3-K2	87	24	5601	774.7	-13.2	0.117
2	45G3-H2	77	19	6623	VP1	78	23	17,505	769.1	-2.2	0.605
3	45G3-K2	32	7	5601	VP1	35	13	17,505	307.9	-1.4	0.685

a ⁱN_{at} indicates the number of interfacing atoms in the corresponding structure

b ⁱN_{res} indicates the number of interfacing residues in the corresponding structure

c Surface Å² is the total solvent accessible surface area in square Ångstroms

d Interface area in Å², calculated as difference in total accessible surface areas of isolated and interfacing structures divided by two

e ΔⁱG indicates the solvation free energy gain upon formation of the interface, in kcal/M

f ΔⁱG P-value indicates the P-value of the observed solvation free energy gain

high-content imaging techniques. (Supplementary Material, Figure S4).

To further confirm the interaction between 45G3 and EMCV and to preliminarily investigate the neutralization mechanism of 45G3, a virus adsorption inhibition assay was conducted. The results showed that 45G3 effectively inhibited the viral adsorption stage, thereby preventing subsequent viral infection. As depicted in Fig. 4B, the viral copy number in the group incubated with EMCV and 45G3 was almost undetectable, whereas the viral copy number in the group incubated with EMCV and mouse IgG reached approximately 10⁶ copies/well. Statistical analysis via a t test revealed a significant difference ($P=0.005$), confirming the marked inhibitory effect of 45G3 on viral attachment (Fig. 4B).

45G3 mAb protected against EMCV infection in BALB/c mice

The neutralization efficacy of the 45G3 monoclonal antibody against EMCV was evaluated. We administered the treatment before and after viral infection to demonstrate the preventive and therapeutic effects of the monoclonal antibody. The mice in groups A (treated 24 h before infection) and C (treated at intervals of 1 h, 24 h, 48 h and 72 h postinfection) presented negligible viral loads across various tissues. In the heart, groups A, C, E and F were significantly different from group D ($P<0.01$), whereas there was no significant difference between groups B and D. In the kidney, groups A, B, C, E and F were significantly different from toxin group D ($P<0.05$). In the brain tissue, groups A and F were significantly different from group D ($P<0.01$), whereas group C was significantly different from group D ($P<0.05$). No significant differences were observed between groups B and D. In the liver, spleen and lung tissues, there were no significant differences between any of the groups and group D (Fig. 5C). These groups also achieved a 100% survival rate over 14 d (Fig. 5B), with their body weights returning to

baseline levels by the end of the study (Fig. 5A). These results demonstrated the potent therapeutic and prophylactic benefits conferred by the 45G3 monoclonal antibody following EMCV exposure. Conversely, mice in group B (treated 24 h after infection) presented brain tissue viral loads similar to those observed in group D (untreated) along with a significant reduction in body weight. However, the progression to onset and mortality in group B were significantly delayed compared with those in the untreated control group. Furthermore, the brain tissue viral load in group E (treated at 24 h and 48 h postinfection) was lower than that in group B. Survival curve analyses revealed postponement of disease onset and mortality by 1 and 2 d, respectively, compared with those in group B and the control group. These findings suggest that even delayed administration of 45G3 can confer partial protection against EMCV, likely because of the high virulence of EMCV at an administered infectious dose of 1×10^6 TCID₅₀ per mouse.

The 45G3 mAb reduces pathological lesions and inflammation in vivo

As shown in Fig. 6A, in group D (the PBS challenge group), numerous areas of coagulative necrosis were observed in the heart. In contrast, group F (healthy control group) exhibited myocardial cells with clear striations, which were arranged in parallel and appeared uniform and orderly. The hearts of groups A (administered 24 h before the challenge) and E (administered 1, 24, 48 and 72 h after the challenge) were consistent with those of the normal control group F. In group D, significant brain edema and inflammatory cell infiltration were noted, whereas those of group F presented normal meninges, a clear cortical structure, and no inflammatory cell infiltration within the white matter. Compared with those in the normal control group, the liver tissue in groups A and E was not significantly different. In group D, the liver tissue exhibited pronounced

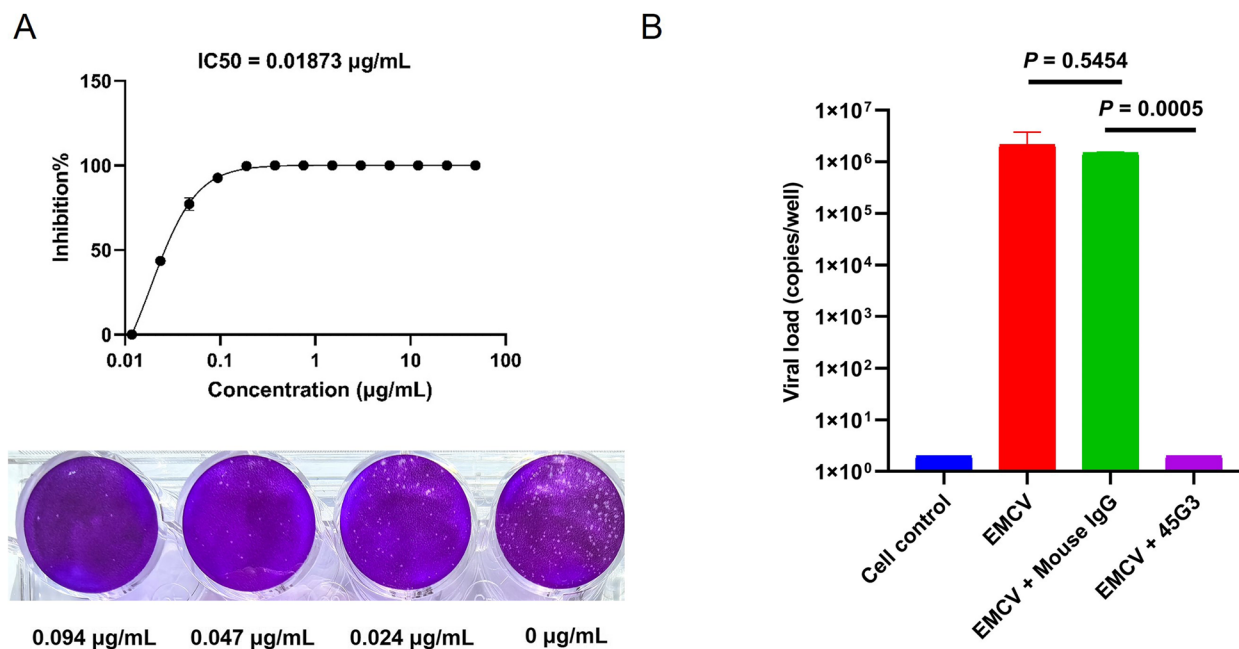


Fig. 4 Detection of neutralizing titers and mechanistic analysis. Note: **A.** IC50 detection of the 45G3 antibody via a plaque reduction neutralization test. The horizontal axis represents the concentration of 45G3, whereas the vertical axis represents the percentage of EMCV inhibition. **B.** 45G3-mediated blockage of viral adsorption. The vertical axis indicates the viral load in the cell supernatant. Cell control: no virus or antibody was present; EMCV: only EMCV was added; EMCV + mouse IgG: EMCV was incubated with mouse IgG; EMCV + 45G3: EMCV was incubated with the 45G3 antibody

fatty degeneration characterized by the accumulation of lipid droplets within hepatocytes, along with significant infiltration of inflammatory cells. In contrast, group F displayed a well-organized hepatic architecture, with hepatocytes arranged in a regular pattern and showing normal morphology. The cellular structure was intact, and no signs of inflammation were observed. Compared with those in group F, the histological appearance of the samples in groups A and E was consistent with that of normal liver tissue. In group D, the kidney tissue exhibited extensive areas of ballooning degeneration. Conversely, group F demonstrated well-preserved renal tubules featuring a distinct brush border and uniform epithelial cells, while the glomeruli maintained their typical structure, showing no evidence of damage or inflammation. Compared with those of Group F, Groups A and E were not significantly different, indicating a

similar histological appearance. In group D, the lung tissue exhibited ventilation obstruction, indicating compromised airflow and potential impairment of gas exchange. In contrast, group F included normal lung tissue characterized by a well-organized structure, with intact alveoli and clear interstitial spaces. No significant abnormalities were observed in groups A and E, which presented histological features consistent with those of group F. In group D, the lung tissue exhibited ventilation obstruction. In contrast, group F included normal lung tissue characterized by a well-organized structure, with intact alveoli and clear interstitial spaces. No significant abnormalities were observed in groups A and E, which presented histological features consistent with those of group F. No significant abnormalities were observed in the spleens of any of the groups.

(See figure on next page.)

Fig. 5 Evaluation of the neutralization capacity of mAbs against EMCVs in vivo. Note: **A.** Monitoring of body weight in different groups for a period of 14 days. **B.** Survival rate of the mice in each group after challenge with EMCV for a period of 14 days; **C.** Viral load in different tissues of the mice, including the heart, liver, spleen, lung, kidney, and brain. The samples were collected over a period of 4 days, and a p value of < 0.05 was considered to indicate statistical significance. As shown in each panel of Fig. 4, Group A received treatment 24 h prior to infection, Group B received treatment 24 h after infection, and Group C underwent treatment at intervals of 1, 24, 48 and 72 h post infection. Group D was challenged with only EMCV, whereas Group E received treatment at 24 and 48 h post infection. Group F served as the control and received only PBS without viral challenge

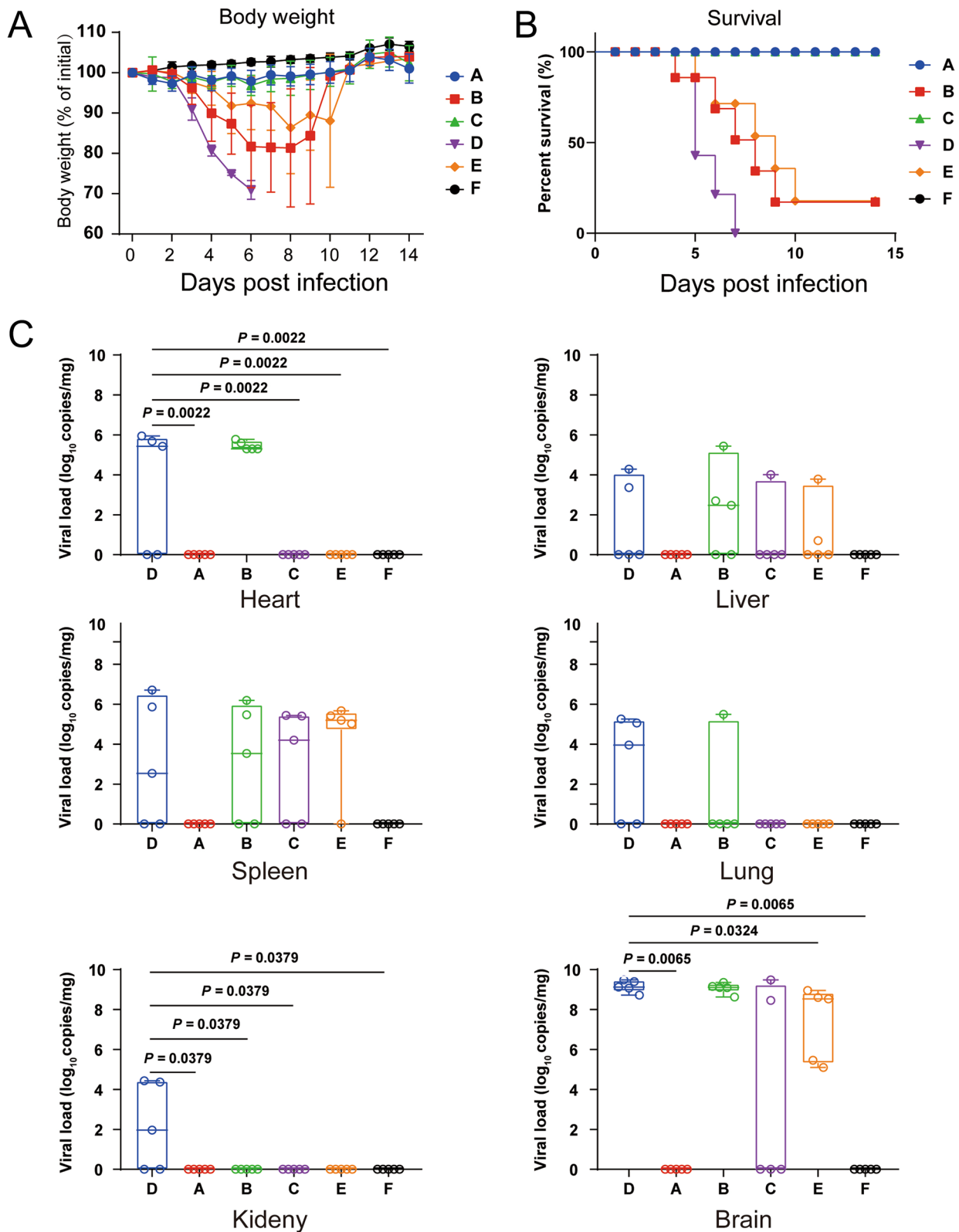


Fig. 5 (See legend on previous page.)

Overall, these findings indicate that the 45G3 antibody can significantly reduce tissue and organ damage in mice and facilitate viral clearance. This finding is consistent with the 100% survival rate observed in the mice. In groups B (1 h and 24 h postinfection) and C (1 h, 24 h and 48 h postinfection), the pathological changes observed in the affected mice were not significantly alleviated (data not shown).

We analyzed multiple inflammatory factors in the brain tissue of mice and found that group D (the virus-challenged group) exhibited significant upregulation of TNF α , CXCL9, CXCL10, IL-6 and IFN- β . The expression levels of CXCL9 in groups A, C, E and F were significantly different from those in group D ($P < 0.05$), whereas those in group B were not different. The expression levels of CXCL10 in groups A, C, E and F were extremely significantly different from those in group D ($P < 0.01$), and those in group B were significantly different ($P < 0.05$). Compared with those in group D, the expression levels of TNF- α in groups A, B, C, E and F significantly differed ($P < 0.001$). The expression levels of IFN- β in groups A and F were extremely significantly different from those in group D ($P < 0.001$), whereas those in group E were significantly different ($P < 0.05$), and those in groups B and C were not significantly different. Compared with those in group D, the expression levels of IL-6 in groups A, C, E and F were extremely significantly different ($P < 0.001$), whereas those in group B were significantly different ($P < 0.05$). These findings suggest that viral infections increase inflammatory responses in the mouse brain. Compared with those in group D, the expression levels of each inflammatory factor in group A were extremely significantly different from those in group D. Compared with those in group D, the continuous therapeutic treatment group E presented a significant decrease in each factor. Groups B and C presented a certain decrease in the expression level of each inflammatory factor compared with that in group E. Following antibody administration, the level of inflammation decreased, possibly because the antibodies impeded virus-induced inflammation, which may have contributed to the improved survival rate of the mice (Fig. 6B).

Discussion

Our results offer significant insights into the development of a novel therapeutic approach against EMCV, a pathogen with notable socioeconomic and health implications across various species. This study successfully produced EMCV-VLPs via a baculovirus expression system, demonstrating their potential as vaccine candidates owing to their strong immunogenicity and safety. These VLPs, which mimic the viral surface, can trigger robust neutralizing antibody responses. Furthermore, VLPs were employed as immunogens to successfully identify an antibody, designated 45G3, that possesses neutralizing capabilities. This approach not only enhances the efficiency of neutralizing antibody identification but also substantiates the potent immunogenicity of VLPs in eliciting robust humoral immune responses, highlighting their potential utility in immunological research and vaccine development.

The successful generation of EMCV-VLPs through the baculovirus expression system represents a significant improvement, given the capacity of VLPs to accurately mimic the viral surface and elicit a strong neutralizing antibody response. This finding aligns with previous research showing the effectiveness of VLP-based vaccines against various Picornaviridae family members, such as enteroviruses (Liu et al. 2023; Wang et al. 2021), polioviruses (Bahar et al. 2022; Sherry et al. 2020), and foot-and-mouth disease viruses (Han et al. 2023). The use of VLPs derived from the P12A and 3C proteins of EMCV as immunogens led to the isolation of the 45G3 monoclonal antibody, which exhibited high specificity toward the conformational epitopes of EMCV, indicating its potential for neutralizing viral activity. The inability of 45G3 to recognize linear epitopes, as evidenced by the failure to reveal any band via WB analysis, further elucidates the specificity of the antibody–epitope interactions. In this study, we were unable to ascertain the specific protein targeted by this antibody. Nonetheless, we employed AlphaFold3 and PDB3PISA, which indicated potential recognition of the VP1 protein. Importantly, this prediction may not accurately reflect the actual binding profile and is accompanied by inherent limitations. Therefore, further experimental validation is essential to confirm

(See figure on next page.)

Fig. 6 Body reactions of the mice in each group post challenge with EMCV. Note: **A.** Histopathological section after challenge. The figure displays the pathological characteristics of various tissues collected on day 4. The regions of pathological changes in the tissue are marked with red arrows in the figure. In heart tissue, the red arrows point to foci of coagulative necrosis. In liver tissue, the red arrows signify areas of fatty change (steatosis). In lung tissue, the red arrows denote the presence of ventilation impairment. In kidney tissue, the red arrows indicate features of ballooning degeneration. In brain tissue, the red arrows point to evidence of cerebral edema. **B.** Expression of inflammatory factors in mouse brain tissue. Group A received treatment 24 h prior to infection, Group B received treatment 24 h after infection, and Group C underwent treatment at intervals of 1, 24, 48 and 72 h post infection. Group D was solely challenged with EMCV, whereas Group E received treatment at 24 and 48 h post infection. Group F served as the control and received only PBS without viral challenge

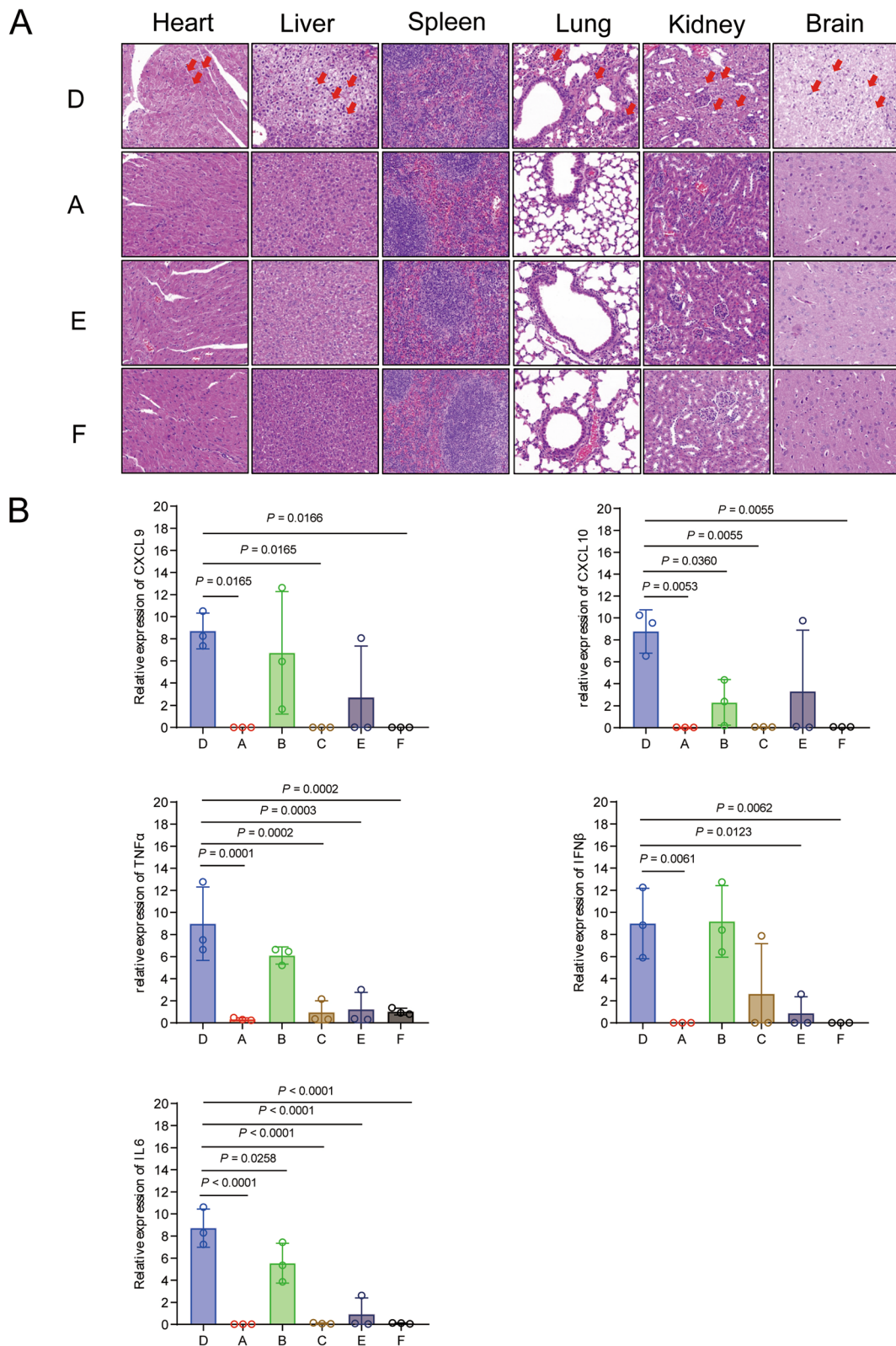


Fig. 6 (See legend on previous page.)

the specificity of an antibody and its potential interactions with VP1 or other related proteins. This specificity is crucial for developing targeted therapies that minimize cross-reactivity and potential off-target effects. *In vitro* and *in vivo* assessments of the neutralizing efficacy of 45G3, particularly its substantial impact on reducing viral loads and improving survival rates in treated mice, highlighted the therapeutic potential of this antibody. These observations are consistent with the growing body of literature emphasizing the importance of monoclonal antibodies in viral disease management owing to their specificity and efficacy; however, the observed variation in therapeutic outcomes on the basis of the timing of antibody administration post infection underscores the necessity for timely intervention to achieve optimal therapeutic effects. The partial protection conferred by the delayed administration of 45G3 suggests that although immediate postexposure treatment is ideal, there is a potential window for therapeutic intervention, even after the onset of infection. This aspect is particularly relevant for managing outbreaks in animal populations where immediate identification and treatment of infected individuals may not always be feasible. This study also highlights the need for further research to optimize dosing strategies and explore the protective efficacy of monoclonal antibodies in a broader context, including different strains of EMCV and across various animal species. This study revealed the development of a monoclonal antibody that exhibited significant neutralization potency both *in vitro* and *in vivo*, underscoring its potential for pharmaceutical development against EMCV. Future studies should focus on humanizing or porcinating the antibody and conducting structural analyses to better understand its mechanism of action and enhance its applicability in therapeutic contexts. This study lays a critical foundation for EMCV prevention and treatment, contributing to the broader field of vaccine development and virus control.

Additionally, the high pathogenicity of EMCV at infectious doses highlights the importance of performing dose-dependent studies to evaluate the efficacy of therapeutic interventions. Histopathological examination revealed a significant reduction in tissue damage across multiple organs in mice treated with the 45G3 antibody. Notably, compared with the untreated control mice, the treated mice presented reduced inflammation and tissue damage in the brain, heart, liver, lungs, and kidneys. The reduction in inflammatory responses and tissue damage likely contributed to the improved survival rates observed in treated mice. Quantitative analysis of inflammatory factors in brain tissue revealed significant upregulation of TNF- α , CXCL9, CXCL10, IL-6 and IFN- β in virus-challenged mice. Treatment with

the 45G3 antibody resulted in a marked reduction in the levels of these inflammatory markers, suggesting that the antibody effectively mitigated virus-induced inflammation. This reduction in inflammation likely plays a crucial role in protecting against tissue damage and in improving survival outcomes. Although this antibody exhibited significant preventive and therapeutic effects in experimental mice, it has not yet been evaluated in porcine models. Future research should focus on modifying antibodies to increase their efficacy for the prevention and treatment of diseases in swine populations. This adaptation will be crucial for translating our findings into practical applications within veterinary medicine. On the basis of the above research, we speculate that EMCV primarily enters the host through the oral or respiratory route, where it can infect cells in the heart, brain, and other organs. During EMCV infection, the host inflammatory response is activated. The release of cytokines, such as IL-6 and TNF- α , along with chemokines, triggers both local and systemic inflammation. Although this inflammatory response can serve as a mechanism for the host to combat the virus, excessive inflammation can lead to tissue damage and pathological changes, potentially resulting in multiorgan failure and death.

Overall, this study contributes significantly to the field of EMCV control and treatment by offering new insights into VLP vaccine development and monoclonal antibody therapy. These findings reinforce the importance of continued research in this area, particularly for understanding the underlying mechanisms of the immunogenicity and protection conferred by these novel biomedical approaches. Future research should consider the scalability and practicality of these methods for their widespread application in EMCV prevention and treatment.

Conclusions

This study advances the development of therapies against EMCV by engineering a baculovirus system to produce EMCV-specific VLPs, leading to the isolation of the monoclonal antibody 45G3. Because of its high specificity and neutralizing activity toward EMCV conformational epitopes, 45G3 has promising therapeutic and prophylactic potential. The *in vivo* efficacy, highlighted by reduced viral loads and enhanced survival of treated mice, underscores the importance of early intervention. Moreover, there was a noticeable reduction in tissue damage and a significant decrease in the inflammatory response in the brain tissue of the mice after treatment, indicating that the 45G3 antibody may have successfully inhibited viral infection, leading to less tissue damage and improved survival rates in the mice. This study paves the way for future antiviral strategies against EMCV, emphasizing the value of mAbs in combating zoonotic pathogens.

Further studies are necessary to optimize the treatment protocols and assess broader applications. Future investigations, potentially involving lower infectious doses, may further elucidate and enhance the protective and therapeutic potential of delayed 45G3 antibody treatment against EMCV infections.

Methods

Cells, viruses and antibodies

A Vero cell line (CCL-81) and an SP2/0 myeloma cell line (PTA-9396) were acquired from the American Type Culture Collection (USA). These cells were propagated in Dulbecco's modified Eagle's medium with a high glucose content (NZK Biotech, China) and enriched with 10% fetal bovine serum (Gibco, Australia). In parallel, *Spo-doptera frugiperda* Sf9 cells were maintained in Grace's insect medium (Gibco, USA), adjusted to a pH of 6.0 and supplemented with 10% FBS at a constant temperature of 27°C. The EMCV strain (GenBank accession number: DQ464062.1) was generously provided by Professor Shu Zhu of Zhejiang University. The secondary antibodies utilized included horseradish peroxidase-conjugated goat anti-mouse immunoglobulin (Ig)G (H+L) (Proteintech group, China) for western blot (WB) analyses and goat anti-mouse IgG H&L conjugated with Alexa Fluor[®] 488 (Abcam, UK) for immunofluorescence assays. Anti-VP1 is a monoclonal antibody generated through a hybridoma cell screening system following the immunization of mice with prokaryotically expressed VP1 protein. This antibody is used in Western blot (WB) and immunofluorescence (IFA) assays.

Generation of the recombinant baculovirus Ac-P12A-3C

The EMCV P12A and 3C genes were engineered into multiple cloning sites under the control of the polyhedrin and P10 promoters within the pFastBac Dual vector, resulting in the creation of the donor plasmid pFastBac-P12A-3C. This plasmid was subsequently introduced into DH10Bac *Escherichia coli* cells. AcBac-P12A-3C recombinant bacmids were selected via blue-white screening. These recombinant bacmids were subsequently transfected into Sf9 insect cells, facilitating the generation of Ac-P12A-3C recombinant baculovirus. This methodological approach ensures the precise insertion of EMCV genes into the baculovirus genome, allowing efficient expression in insect cell lines, which is critical for the production of viral proteins for further research and vaccine development purposes (Fig. 1A).

Production and purification of EMCV-VLPs

Before initiation of the experiment, Sf9 cells were cultured in flasks and seeded at an initial concentration of 1×10^7 cells/mL. When cell proliferation reached a

confluence exceeding 80%, the cells were infected with Ac-P12A-3C recombinant baculovirus at a multiplicity of infection of 1. The infection period spanned 48–72 h, after which both the supernatant and the cell pellets were carefully harvested for further evaluation.

After 72 h of infection, Sf9 cells harboring Ac-P12A-3C were harvested and centrifuged at $2000 \times g$ for 10 min. The collected pellets were resuspended and washed with PBS, followed by an additional centrifugation step under identical conditions. The cells were then lysed *via* a Tissue Cell Destroyer 1000 (NZK Biotech, China) at 4500 rpm for 10 s, and the resulting lysate was further centrifuged at $9,000 \times g$ for 30 min to separate the supernatant. The supernatant was carefully layered over a discontinuous CsCl gradient (1.2 g/cm^3 and 1.4 g/cm^3) in SW41 ultracentrifuge tubes and centrifuged at 36,000 rpm for 2 h. The intermediate white layer rich in EMCV-VLPs was extracted, diluted with prefiltered PBS, and centrifuged at 20,000 rpm for 2 h. The purified pellet containing the VLPs was resuspended in PBS for further analysis.

Detection of EMCV-VLPs by transmission electron microscopy (TEM)

Sf9 cells infected with the Ac-P12A-3C virus for 72 h were subjected to a series of treatments, including fixation, dehydration, embedding, infiltration, sectioning, and staining. The morphological characteristics of the viral particles were observed *via* transmission electron microscopy at 200 kV. For purified EMCV-VLPs and wild-type EMCV, we performed negative staining as described below. The purified EMCV-VLP sample (10 μL) was applied to a copper grid and allowed to adsorb for 2 min. The sections were then stained with phosphotungstic acid for 1 min and air-dried. The morphology of the VLPs was examined under an electron microscope, which enabled detailed visualization of the particle structure.

Hybridoma generation and screening

Purified EMCV-VLPs were emulsified with an equal volume of Freund's adjuvant by vigorous shaking. Five female BALB/c mice, aged 6–8 weeks and of specific pathogen-free status, were selected for a series of subcutaneous immunizations. The immunization regimen consisted of three doses administered at 2-week intervals, with each mouse receiving a 100 μg dose. Before each immunization, orbital blood samples were collected to analyze the elicited immune responses.

Following immunization, booster doses were administered intraperitoneally. After 3 d, orbital blood was collected, and the mice were euthanized. The spleens were aseptically harvested and processed in RPMI-1640

medium to prepare splenocyte suspensions. This suspension was mixed with myeloma cells at a ratio of 5:1, followed by polyethylene glycol-mediated cell fusion. The fused cells were cultured in HAT-supplemented medium in a CO₂ incubator. After 10 d, cell colonies were assessed for EMCV-specific antibody production *via* immunofluorescence and neutralizing antibody assays. This procedure facilitated the isolation of hybridoma cells that secreted EMCV-specific neutralizing antibodies, which were subsequently screened to establish stable monoclonal cell lines.

Plaque reduction neutralization assay

To determine the neutralizing potency of the selected monoclonal 45G3 cell line, 45G3 monoclonal antibodies were first diluted to concentrations of 0.012, 0.024, 0.047, 0.094, 0.189, 0.377, 0.755, 1.509, 3.019, 6.038, 12.075, 24.150 and 48.300 µg/mL. The EMCV was then diluted to 100 PFU/mL and mixed with diluted monoclonal antibodies in equal volumes. After incubation at 37 °C for 1 h, the mixture was added to BHK cells in a 12-well plate. After incubation at 37 °C for 1 h, the supernatant was removed, and 1 mL of MEM containing 2% FBS and 0.9% methylcellulose was added to each well. The cells were then incubated at 37 °C with 5% CO₂ for 24 h. Following incubation, 4% paraformaldehyde was added for 1 h to fix the cells. The supernatant was discarded, and the wells were washed 2–3 times with water. The cells were then stained with 0.5% crystal violet for 10 min. Plaque counts were recorded, and the half-maximal inhibitory concentration (IC₅₀) values were calculated. All the experiments were conducted in triplicate.

Prediction of antibody binding to EMCV capsid proteins via AlphaFold3 and PDB3PISA

To predict the potential binding of the 45G3 antibody to individual EMCV capsid proteins (VP1, VP2, VP3 and VP4), a computational approach combining AlphaFold3 (<https://alphafoldserver.com/>) and PDB3PISA was employed. The full-length sequences of the four EMCV capsid proteins were submitted to the AlphaFold3 server for three-dimensional structure prediction (Abramson et al. 2024). Models were evaluated on the basis of predicted local distance difference test (pLDDT) scores, with only those scoring above 90 considered for further analysis. For each capsid protein, the structure of 45G3 was either retrieved from experimental data or predicted via AlphaFold3 if unavailable. Molecular docking of 45G3 to the predicted structure of each capsid protein was performed via the PDB3PISA server, which facilitates the analysis of protein–protein interactions and the prediction of potential binding interfaces on the basis of steric compatibility and interaction energy scores (Krissinel

and Henrick 2007). The docking results were assessed on the basis of the predicted binding affinity, interface size, and interaction energy between the 45G3 antibody and each capsid protein. The most likely binding model for each capsid protein was selected on the basis of the lowest binding energy and the most favorable interaction surface. Interaction patterns were analyzed to identify key residues involved in antibody–protein binding, providing insights into the specificity of the 45G3 antibody for individual capsid proteins. However, this method has certain limitations and may not accurately reflect the true structural characteristics.

Immunsorbent electron microscopy (IEM)

To investigate the direct interaction between the 45G3 monoclonal antibody and encephalomyocarditis virus (EMCV), we employed immunoelectron microscopy (IEM) alongside viral supernatant collection and ultracentrifugation. Vero cells were cultured and infected with EMCV at a multiplicity of infection (MOI) of 0.1. At 24 h post infection, the viral supernatant was collected and clarified by centrifugation at 2,000×g for 10 min to remove cell debris. The supernatant was then subjected to ultracentrifugation at 100,000×g for 1 h to concentrate the virus particles. Following ultracentrifugation, the pelleted virus was resuspended in phosphate-buffered saline (PBS) for subsequent immunolabeling. Concentrated EMCV particles were incubated with either the 45G3 antibody (1:100 dilution) or a mouse IgG isotype control (1:100 dilution) for 1 h at room temperature. After being washed with PBS containing 0.1% Tween-20 to remove unbound antibodies, the samples were incubated with 6 nm gold-conjugated goat anti-mouse IgG (1:50 dilution) for 1 h. The samples were washed again, stained with 2% uranyl acetate for 10 min, and subsequently treated with lead citrate for 5 min to enhance contrast. The labeled samples were examined via transmission electron microscopy (TEM) at 200 kV, and images were captured at various magnifications.

45G3 antibody blocking adsorption assay

To further explore the neutralization mechanism of neutralizing antibodies, a 24-well plate was prepared in this study, with various cell types seeded at a density of 1.25×10^5 cells per well. At least three replicates were included for each cell type to facilitate subsequent RNA extraction. For the cell binding assay, 200 µg of the 45G3 antibody and mouse IgG were mixed separately with EMCV at a multiplicity of infection (MOI) of 1 and incubated at 37 °C for 1 h. Simultaneously, controls for both the virus and the cells were set up. After incubation, the mixtures were added to the cells, which

were then placed in a P2 refrigerator at 4°C for an additional hour. Following this incubation, the cells were washed three times with cold phosphate-buffered saline (PBS) to remove any unbound virus. Finally, 300 µL of TRIzol was collected for sample preparation, and the samples were subsequently subjected to RNA extraction and quantitative PCR (qPCR) analysis to assess viral binding.

In vivo animal experiments

An in vivo study was designed to evaluate the protective efficacy of the 45G3 mAb in mice (BALB/c, 6–8-week-old, female) distributed into six groups, with treatments administered via intraperitoneal injection of approximately 30 mg/kg mAb or PBS as a control. All the groups were challenged with a dose of 1×10^6 TCID₅₀ per mouse. Group A received treatment 24 h before infection, whereas group B received treatment 24 h after infection. Group C received treatment at 1, 24, 48 and 72 h post infection. Group D was only challenged with EMCV, whereas group E was treated at 24 h and 48 h post infection. Group F served as the control and received only PBS without viral challenge. Changes in body weight and survival were monitored for 14 d. On days 4 and 14 postchallenge, the mice were sacrificed, and the liver, spleen, lungs, and kidneys were harvested for viral load analysis and fixed in 4% paraformaldehyde for tissue sectioning. Mouse tissue sectioning and hematoxylin and eosin staining were performed as previously described (Shen et al. 2022).

RNA Extraction

For RNA extraction, 1 mL of PBS was added to the pre-weighed tissue sample. The sample was homogenized twice via a Tissue Cell Destroyer 1000 (NZK Biotech, China) at 4,500 rpm for 10 s. A volume of 0.2 mL of homogenized tissue was mixed with 0.8 mL of RNAiso Plus (Takara, Japan). The procedure was subsequently carried out according to the RNA Iso Plus protocol. The concentration and purity of the extracted RNA were assessed via a NanoDrop microvolume spectrophotometer (Thermo Fisher Scientific, USA).

Fluorescence quantitative polymerase chain reaction (PCR) detection

For fluorescence quantitative PCR detection, the following primers and probes for EMCV reverse transcription (RT)-PCR were designed: forward primer (EMCV-3D-F): 5'-TGACCCTAGAACAGAGGCTGATG-3'; reverse primer (EMCV-3D-R): 5'-GGTGTTCCTGTCCATGGG GTC-3'; and probe (EMCV-3D-P): FAM-CCAACCAGG

AAAGCCTCCCACCAG-BHQ1. Standard samples were prepared by serially diluting the initial concentration to 10^8 copies/µL to establish a calibration curve. Fluorescence RT-PCR was conducted via the One Step PrimeScript™ RT-PCR Kit (Perfect Real Time) (Takara, Japan) according to the one-step protocol. The procedure was performed on a CFX96-touch (Bio-Rad) fluorescence PCR system, adhering to the protocol provided by the One Step PrimeScript™ RT-PCR Kit (Perfect Real Time) (Takara, Japan). To determine the quantity of tissue nucleic acid utilized for PCR detection in various tissues, we employed a standard curve and referenced the copy numbers of standard samples. Subsequently, leveraging the established relationship between the mass and the aliquoted volume of each tissue, we calculated the copy number per unit mass. The expression of inflammatory factors, such as TNF-α, CXCL9, CXCL10, IL-6 and IFN-β, in mouse brain tissue was detected as reported in the literature (Hu et al. 2022; Zhang et al. 2020).

Abbreviations

EMCV	Encephalomyocarditis Virus
FBS	Fetal Bovine Serum
PBS	Phosphate-Buffered Saline
PCR	Polymerase Chain Reaction
TEM	Transmission Electron Microscopy
VLP	Virus-like Particle

Supplementary Information

The online version contains supplementary material available at <https://doi.org/10.1186/s44149-024-00154-7>.

- Supplementary Material 1.
- Supplementary Material 2.
- Supplementary Material 3.
- Supplementary Material 4.

Acknowledgements

We would like to thank Pei Zhang, Bichao Xu and Anna Du from the Center for Instrumental Analysis and Metrology, Wuhan Institute of Virology, Chinese Academy of Sciences, for their technical support in transmission electron microscopy.

Authors' contributions

YFZ, FD and SBC conceived and designed the experiments; YFZ and ZYW screened mAbs; YFZ identified and completed antibody evaluations at the cellular and animal levels; YFZ and JF completed the nucleic acid assay in animal tissues. SS, QZ, JYJ, SWH, and SJH assisted the animal experiments; YJ, MZ, DNZ, YLD, LLX, XJL and LLX assisted in the cell experiments; YFZ and YHF wrote the manuscript; and SS, FD and SBC revised the manuscript. All authors approved the final version of the manuscript.

Funding

This research is funded by the National Key Research and Development Program of China (grant number: 2023YFC2306501) and the Hubei Provincial Fund for Supporting High-Quality Development of the Seed Industry "Conservation and Utilization of Agricultural Germplasm Resources" Project (grant number: HBZY2023A001-16).

Data availability

Data will be shared upon request by the readers.

Declarations

Ethics approval and consent to participate

The animal experiments were approved by the ethics committee of Wuhan Institute of Virology, Chinese Academy of Sciences, under the approval number WIVA33202109.

Competing interests

No potential competing interests were reported by the authors. Author Shengbo Cao was not involved in the journal's review or decisions related to this manuscript.

Author details

¹National Key Laboratory of Agricultural Microbiology, Huazhong Agricultural University, Wuhan, Hubei, China. ²Frontiers Science Center for Animal Breeding and Sustainable Production, Huazhong Agricultural University, Wuhan, Hubei 430070, People's Republic of China. ³The Cooperative Innovation Center for Sustainable Pig Production, Huazhong Agricultural University, Wuhan, Hubei, China. ⁴Hubei Hongshan Laboratory, Wuhan, Hubei 430070, People's Republic of China. ⁵Key Laboratory of Virology and Biosafety and National Virus Resource Center, Wuhan Institute of Virology, Chinese Academy of Sciences, Wuhan, Hubei 430071, China.

Received: 21 August 2024 Accepted: 21 December 2024

Published online: 23 January 2025

References

- Abramson, J., J. Adler, J. Dunger, R. Evans, T. Green, A. Pritzel, O. Ronneberger, L. Willmore, A.J. Ballard, J. Bambrick, et al. 2024. Accurate structure prediction of biomolecular interactions with AlphaFold 3. *Nature* 630 (8016): 493–500. <https://doi.org/10.1038/s41586-024-07487-w>.
- An, D.J., W. Jeong, H.Y. Jeoung, S.H. Yoon, H.J. Kim, C.U. Choi, and B.K. Park. 2009. Encephalomyocarditis in Korea: Serological survey in pigs and phylogenetic analysis of two historical isolates. *Veterinary Microbiology* 137 (1–2): 37–44. <https://doi.org/10.1016/j.vetmic.2009.01.005>.
- Bahar, M.W., V. Nasta, H. Fox, and L. Sherry. 2022. A conserved glutathione binding site in poliovirus is a target for antivirals and vaccine stabilization. *Communications Biology* 5 (1): 1293. <https://doi.org/10.1038/s42003-022-04252-5>.
- Billinis, C. 2009. Encephalomyocarditis virus infection in wildlife species in Greece. *Journal of Wildlife Diseases* 45 (2): 522–526. <https://doi.org/10.7589/0090-3558-45.2.522>.
- Camp, J.V., Desvars-Larrive, A. 2022. Monitoring urban zoonotic virus activity: Are city rats a promising surveillance tool for emerging viruses? *Viruses* 14 (7). <https://doi.org/10.3390/v14071516>.
- Canelli, E., A. Luppi, A. Lavazza, D. Lelli, E. Sozzi, A.M. Martin, D. Gelmetti, E. Paschetto, C. Sandri, W. Magnone, and P. Cordioli. 2010. Encephalomyocarditis virus infection in an Italian zoo. *Virology Journal* 7: 64. <https://doi.org/10.1186/1743-422x-7-64>.
- Cardeti, G., V. Mariano, C. Eleni, M. Aloisi, G. Grifoni, S. Sittinieri, G. Dante, V. Antognetti, E. A. Foglia, A. Cersini, and A. Nardi. 2016. Encephalomyocarditis virus infection in *Macaca sylvanus* and *Hystrix cristata* from an Italian rescue center for wild and exotic animals. *Virology Journal* 13 (1): 193. <https://doi.org/10.1186/s12985-016-0653-9>.
- Carocci, M., and L. Bakkali-Kassimi. 2012. *The Encephalomyocarditis Virus*. *Virulence* 3 (4): 351–367. <https://doi.org/10.4161/viru.20573>.
- Carocci, M., N. Cordonnier, H. Huet, A. Romey, A. Relmy, K. Gorna, S. Blaise-Boisseau, S. Zientara, and L.B. Kassimi. 2011. Encephalomyocarditis virus 2A protein is required for viral pathogenesis and inhibition of apoptosis. *Journal of Virology* 85 (20): 10741–10754. <https://doi.org/10.1128/jvi.00394-11>.
- Cherry, S., 2019. Encephalomyocarditis virus entry unveiled. *mBio* 10 (2). <https://doi.org/10.1128/mBio.00305-19>.
- Czechowicz, J., Huaman, J.L., Forshey, B.M., Morrison, A.C., Castillo, R., Huaman, A., Caceda, R., Eza, D., Rocha, C., Blair, P.J., Olson, J.G., Kochel, T.J., 2011. Prevalence and risk factors for encephalomyocarditis virus infection in Peru. *Vector borne and zoonotic diseases (Larchmont, N.Y.)* 11 (4), 367–374. <https://doi.org/10.1089/vzbz.2010.0029>.
- Dea, S., Bilodeau, R., Sauvageau, R., Martineau, G.P., 1991. Outbreaks in Quebec pig farms of respiratory and reproductive problems associated with encephalomyocarditis virus. *Journal of veterinary diagnostic investigation : official publication of the American Association of Veterinary Laboratory Diagnosticians, Inc.* 3 (4), 275–282. <https://doi.org/10.1177/104063879100300401>.
- Feng, R., J. Wei, H. Zhang, J. Fan, X. Li, D. Wang, J. Xie, Z. Qiao, M. Li, J. Bai, and Z. Ma. 2015. National serosurvey of encephalomyocarditis virus in healthy people and pigs in China. *Archives of Virology* 160 (12): 2957–2964. <https://doi.org/10.1007/s00705-015-2591-z>.
- Foglia, E.A., G. Pezzoni, P. Bonilauri, D. Torri, S. Grazioli, and E. Brocchi. 2023. A recent view about encephalomyocarditis virus circulating in compartmentalized animal population in Northern Italy. *Science and Reports* 13 (1): 592. <https://doi.org/10.1016/j.virusres.2018.10.020>.
- Gainer, J.H. 1967. Encephalomyocarditis virus infections in Florida, 1960–1966. *Journal of the American Veterinary Medical Association* 151 (4): 421–425. <https://doi.org/10.1038/s41598-023-27828-5>.
- Ge, X., D. Zhao, C. Liu, F. Wang, X. Guo, and H. Yang. 2010. Seroprevalence of encephalomyocarditis virus in intensive pig farms in China. *The Veterinary Record* 166 (5): 145–146. <https://doi.org/10.1136/vr.b4766>.
- Gelmetti, D., A. Meroni, E. Brocchi, F. Koenen, and G. Cammarata. 2006. Pathogenesis of encephalomyocarditis experimental infection in young piglets: A potential animal model to study viral myocarditis. *Veterinary Research* 37 (1): 15–23. <https://doi.org/10.1051/vetres:2005041>.
- Guo, C., D. Reus, J. D. Coey, S. Sukumar, B. Lang, J. Mclauchlan, S. Boulant, M. L. Stanifer, and C. G. Bamford. 2021. Conserved Induction of Distinct Antiviral Signalling Kinetics by Primate Interferon Lambda 4 Proteins. *Front Immunol* 12:772588. <https://doi.org/10.3389/fimmu.2021.772588>.
- Han, Y., Xie, J., Xu, S., Bi, Y., Li, X., Zhang, H., Idris, A., Bai, J., Feng, R., 2021. Encephalomyocarditis virus abrogates the interferon beta signaling pathway via its structural protein VP2. *Journal of virology* 95 (6). <https://doi.org/10.1128/jvi.01590-20>.
- Han, R., Liang, L., Qin, T., Xiao, S., Liang, R., 2022. Encephalomyocarditis virus 2A protein inhibited apoptosis by interaction with annexin A2 through JNK/c-Jun pathway. *Viruses* 14 (2). <https://doi.org/10.3390/v14020359>.
- Han, W., Zhang, J., Li, M., An, M., Li, L., 2023. Analysis of chromatin accessibility changes induced by BMMC recognition of foot-and-mouth disease virus-like particles through ATAC-seq. *International journal of molecular sciences* 24 (23). <https://doi.org/10.3390/ijms242317044>.
- Helwig, F.C., Schmidt, C.H., 1945. A filter-passing agent producing interstitial myocarditis in anthropoid apes and small animals. *Science (New York, N.Y.)* 102 (2637), 31–33. <https://doi.org/10.1126/science.102.2637.31>.
- Hu, S., Zha, Y., Yang, W., Cui, K., 2022. Dysregulation of NK and CD8(+)T Cells by the microbiota promotes the progression of lung cancer. 2022 7057089. <https://doi.org/10.1155/2022/7057089>.
- Huang, L., T. Xiong, H. Yu, Q. Zhang, K. Zhang, C. Li, L. Hu, Y. Zhang, L. Zhang, Q. Liu, S. Wang, X. He, Z. Bu, X. Cai, S. Cui, J. Li, and C. Weng. 2017. Encephalomyocarditis virus 3C protease attenuates type I interferon production through disrupting the TANK-TBK1-IKKe-IRF3 complex. *The Biochemical Journal* 474 (12): 2051–2065. <https://doi.org/10.1042/bcj20161037>.
- Krissinel, E., and K. Henrick. 2007. Inference of macromolecular assemblies from crystalline state. *Journal of Molecular Biology* 372 (3): 774–797. <https://doi.org/10.1016/j.jmb.2007.05.022>.
- Liu, H., X. He, X. Song, L. Xu, Y. Zhang, G. Zhou, W. Zhu, C. Chang, Z. Yin, Y. Shi, C. Wang, and H. Chang. 2016. Isolation and molecular and phylogenetic analyses of encephalomyocarditis virus from wild boar in central China. *Infection, Genetics and Evolution* 40: 67–72. <https://doi.org/10.1016/j.meegid.2016.02.025>.
- Liu, X., H. Zhu, M. Wang, N. Zhang, J. Wang, W. Tan, G. Wu, P. Yu, H. Liu, and Q. Liu. 2023. An enterovirus A71 virus-like particle with replaced loops confers partial cross-protection in mice. *Virus Research* 337: 199235. <https://doi.org/10.1016/j.virusres.2023.199235>.
- Luo, Y. K., L. Liang, Q. H. Tang, L. Zhou, L. J. Shi, Y. Y. Cong, W. C. Lin, and S. J. Cui. 2017. Isolation and characterization of encephalomyocarditis virus from dogs in China. *Science and Reports* 7 (1): 438. <https://doi.org/10.1038/s41598-017-00435-x>.
- Medkour, H., S. Castaneda, I. Amona, F. Fenollar, C. André, R. Belais, P. Mungongo, J.J. Muyembé-Tamfum, A. Levasseur, et al. 2021. Potential zoonotic pathogens hosted by endangered bonobos. *Science and Reports* 11 (1): 6331. <https://doi.org/10.1038/s41598-021-85849-4>.

- Mohana Subramanian, B., M. Madhanmohan, R. Sriraman, R.V. Chandrasekhar Reddy, S. Yuvaraj, K. Manikumar, S. Rajalakshmi, S.B. Nagendrakumar, S.K. Rana, and V.A. Srinivasan. 2012. Development of foot-and-mouth disease virus (FMDV) serotype O virus-like-particles (VLPs) vaccine and evaluation of its potency. *Antiviral Research* 96 (3): 288–295. <https://doi.org/10.1016/j.antiviral.2012.09.019>.
- Murnane, T.G., Craighead, J.E., Mondragon, H., Shelokov, A., 1960. Fatal disease of swine due to encephalomyocarditis virus. *Science (New York, N.Y.)* 131 (3399), 498–499. <https://doi.org/10.1126/science.131.3399.498>.
- O'Connor, T. W., D. S. Finlaison, L. K. Manning, M. S. Hazelton, Z. B. Spiers, P. Pinczowski, E. M. Bolin, P. D. Kemsley, N. U. Horadagoda, A. J. Dart, et al. 2020. Encephalomyocarditis virus infection in alpacas. *Australian Veterinary Journal* 98 (10): 486–490. <https://doi.org/10.1111/avj.12962>.
- Palmenberg, A.C., E.M. Kirby, M.R. Janda, N.L. Drake, G.M. Duke, K.F. Potratz, and M.S. Collett. 1984. The nucleotide and deduced amino acid sequences of the encephalomyocarditis viral polyprotein coding region. *Nucleic Acids Research* 12 (6): 2969–2985. <https://doi.org/10.1093/nar/12.6.2969>.
- Reddacliff, L.A., P.D. Kirkland, W.J. Hartley, and R.L. Reece. 1997. Encephalomyocarditis virus infections in an Australian zoo. *Journal of Zoo and Wildlife Medicine: Official Publication of the American Association of Zoo Veterinarians* 28 (2): 153–157.
- Romey, A., Lamglait, B., Blanchard, Y., Touzain, F., Quenault, H., Relmy, A., Zientara, S., Blaise-Boisseau, S., Bakkali-Kassimi, L., 2021. Molecular characterization of encephalomyocarditis virus strains isolated from an African elephant and rats in a French zoo. *Journal of veterinary diagnostic investigation: official publication of the American Association of Veterinary Laboratory Diagnosticians, Inc.* 33 (2), 313–321. <https://doi.org/10.1177/1040638720978389>.
- Salogni, C., Lazzaro, M., Giacomini, E., Giovannini, S., Zannoni, M., Giuliani, M., Ruggeri, J., Pozzi, P., Pasquali, P., Boniotti, M.B., Alborali, G.L., 2016. Infectious agents identified in aborted swine fetuses in a high-density breeding area: a three-year study. *Journal of veterinary diagnostic investigation: official publication of the American Association of Veterinary Laboratory Diagnosticians, Inc.* 28 (5), 550–554. <https://doi.org/10.1177/1040638716656024>.
- Shen, S., Y. Zhang, Z. Yin, Q. Zhu, J. Zhang, T. Wang, Y. Fang, X. Wu, Y. Bai, S. Dai, X. Liu, J. Jin, S. Tang, J. Liu, M. Wang, Y. Guo, and F. Deng. 2022. Antiviral activity and mechanism of the antifungal drug, anidulafungin, suggesting its potential to promote treatment of viral diseases. *BMC Medicine* 20 (1): 359. <https://doi.org/10.1186/s12916-022-02558-z>.
- Sherry, L., Grehan, K., Snowden, J.S., Knight, M.L., Adeyemi, O.O., Rowlands, D.J., Stonehouse, N.J., 2020. Comparative molecular biology approaches for the production of poliovirus virus-like particles using pichia pastoris. *mSphere* 5 (2). <https://doi.org/10.1128/mSphere.00838-19>.
- Tang, H., Y. Ke, Y. Liao, Y. Bian, Y. Yuan, Z. Wang, L. Yang, H. Ma, T. Sun, B. Zhang, X. Zhang, M. Wu, and J. Zhu. 2022. Mutational escape prevention by combination of four neutralizing antibodies that target RBD conserved regions and stem helix. *Viral Sin* 37 (6): 860–873. <https://doi.org/10.1016/j.virs.2022.11.005>.
- Vansteenkiste, K., T. Van Limbergen, R. Decaluwé, M. Tignon, B. Cay, and D. Maes. 2016. Clinical problems due to encephalomyocarditis virus infections in two pig herds. *Porcine Health Manag* 2: 19. <https://doi.org/10.1186/s40813-016-0036-z>.
- Vyshemirskii, O.I., A.A. Agumava, A.A. Kalaydzyan, A.V. Leontyuk, J.H. Kuhn, A.M. Shchetinin, T.V. Vishnevskaya, A.A. Eremyan, and S.V. Alkhovsky. 2018. Isolation and genetic characterization of encephalomyocarditis virus 1 from a deceased captive hamadryas baboon. *Virus Research* 244: 164–172. <https://doi.org/10.1016/j.virusres.2017.11.001>.
- Wang, Z., C. Zhou, F. Gao, Q. Zhu, Y. Jiang, X. Ma, Y. Hu, L. Shi, X. Wang, C. Zhang, B. Liu, L. Shen, Q. Mao, and G. Liu. 2021. Preclinical evaluation of recombinant HFMD vaccine based on enterovirus 71 (EV71) virus-like particles (VLP): Immunogenicity, efficacy and toxicology. *Vaccine* 39 (31): 4296–4305. <https://doi.org/10.1016/j.vaccine.2021.06.031>.
- Wang, R., C. Zhang, Y. Zhang, J. Wu, Y. Zhang, L. Zhang, R. Yu, and Y. Liu. 2023. Synergetic interaction of capsid proteins for virus-like particles assembly of foot-and-mouth disease virus (serotype O) from the inclusion bodies. *Protein Expression and Purification* 204: 106231. <https://doi.org/10.1016/j.pep.2023.106231>.
- Zhang, Z.D., Xiong, T.C., Yao, S.Q., Wei, M.C., Chen, M., Lin, D., 2020. RNF115 plays dual roles in innate antiviral responses by catalyzing distinct ubiquitination of MAVS and MITA. *Virus Res* 11 (1), 5536. <https://doi.org/10.1038/s41467-020-19318-3>.
- Zoll, J., F.J. Van Kuppeveld, J.M. Galama, and W.J. Melchers. 1998. Genetic analysis of mengovirus protein 2A: Its function in polyprotein processing and virus reproduction. *The Journal of General Virology* 79 (Pt 1): 17–25. <https://doi.org/10.1099/0022-1317-79-1-17>.

Publisher's Note

Springer Nature remains neutral with regard to jurisdictional claims in published maps and institutional affiliations.